

Westerly wind events and precipitation in the eastern Indian Ocean as predictors for El Niño: Climatology and case study for the 2002–2003 El Niño

Scott Curtis,¹ Robert F. Adler,² George J. Huffman,³ and Guojun Gu⁴

Received 19 February 2004; revised 24 June 2004; accepted 6 August 2004; published 19 October 2004.

[1] This study expands on recent work linking intraseasonal-to-seasonal variability in observed precipitation and wind from September to March in the eastern Indian Ocean with the initiation of El Niño events during the last 25 years. First, westerly wind burst (WWB) events are defined as days when westerly wind speeds averaged over 5°–15°S and 70°–100°E were greater than 1.5 standard deviations from the mean. The number of WWB days from September to March was high before the onset of the 1982–1983, 1991–1992, 1997–1998, and 2002–2003 El Niño events, but not the 1986–1987 El Niño. This study suggests that for the 1979–2002 period, variations in precipitation in the eastern Indian Ocean is a more robust predictor of El Niño onset than analyzed winds. On the basis of the work of *Curtis et al.* [2002], a real-time precipitation-based El Niño Onset Index is presented, which during the austral summer of 2001–2002 successfully predicted the 2002–2003 El Niño. The index focuses on the magnitude of 30–60 day oscillations and mean conditions in the precipitation field. Case studies of high-resolution satellite-based data sets of precipitation, wind, and sea surface temperature (SST) for the 2001–2002 season are examined to better understand how events in the Indian Ocean are linked to Pacific Ocean wind disturbances and SST changes. Twice during this season maxima in precipitation and zonal winds propagated eastward, the first near the equator and the second to the south. For the southern case, warm waters preceded heavy precipitation in the eastern Indian Ocean, which preceded strong westerly winds. A cooling of the sea surface followed the wind-rain system. This sequence of events moved through the ocean passage between Indonesia and Australia, suggesting a coupling of convection, wind, and sea surface temperatures on the timescale of days. These case studies provide a basis for how the east Indian Ocean variations are linked to subsequent events in the Pacific Ocean, including the initiation of El Niño events. **INDEX TERMS:** 3360 Meteorology and Atmospheric Dynamics: Remote sensing; 3359 Meteorology and Atmospheric Dynamics: Radiative processes; 3354 Meteorology and Atmospheric Dynamics: Precipitation (1854); 4522 Oceanography: Physical: El Niño; **KEYWORDS:** precipitation, El Niño, onset

Citation: Curtis, S., R. F. Adler, G. J. Huffman, and G. Gu (2004), Westerly wind events and precipitation in the eastern Indian Ocean as predictors for El Niño: Climatology and case study for the 2002–2003 El Niño, *J. Geophys. Res.*, 109, D20104, doi:10.1029/2004JD004663.

1. Introduction

[2] There is an ongoing debate as to the usefulness of wind observations in predicting the development of El Niño events. Recent papers have argued whether or not the Madden-Julian Oscillation (MJO) [*Madden and Julian, 1994*] and/or westerly wind burst events act as a stochastic

forcing for El Niño [e.g., *Kessler and Kleeman, 2000; Vecchi and Harrison, 2000; Zhang and Gottschalck, 2002; Fedorov, 2002; Fedorov et al., 2003; Belamari et al., 2003*]. Many of these studies have concentrated on the western Pacific. However, recently intraseasonal convective anomalies associated with the MJO have been tracked from the Indian Ocean to the western Pacific [*Jones et al., 2004*]. Using a coarse 5° × 5°-resolution outgoing longwave radiation (OLR) data set as a proxy for convection, these authors did not find a significant relation between the MJO and the phases of El Niño/Southern Oscillation, although there was an enhancement of western Pacific wind speeds. However, *Krishnamurti et al.* [2000] suggest important teleconnections between the phase and amplitude of zonal winds over the near-equatorial southern Indian Ocean and the subsequent onset of El Niño events.

¹Department of Geography, East Carolina University, Greenville, North Carolina, USA.

²NASA Goddard Space Flight Center, Greenbelt, Maryland, USA.

³Science Systems and Applications, Inc., Greenbelt, Maryland, USA.

⁴Goddard Earth Science and Technology Center, University of Maryland Baltimore County, Baltimore, Maryland, USA.

[3] A seasonally averaged westerly wind signal has also been observed in the eastern Indian Ocean more than a season before the onset of El Niño [Gutzler and Harrison, 1987; Harrison and Larkin, 1998]. In that respect, Clarke and Van Gorder [2003] improved their El Niño prediction, in part, by extending the equatorial zonal wind stress anomaly used to construct their predictor to the central Indian Ocean. However, wind alone has been an insufficient predictor for El Niño. For example, Clarke and Van Gorder [2003] also add ocean indices to improve their predictions. What Gutzler and Harrison [1987] postulated nearly two decades ago still rings true: a complicated combination of atmospheric and oceanic conditions are necessary for an El Niño to occur.

[4] Unfortunately, today the coverage of in situ sea surface observations remains limited. High-quality daily values of wind and sea surface temperature (SST) can be obtained from buoys over the Pacific (TRITON/TAO). McPhaden [2004] used this data to investigate the onset of the 2002–2003 El Niño. TRITON/TAO data are routinely assimilated into climate models, which can be used to construct reliable climatologies of subseasonal variability since the mid-1980s [Harrison and Vecchi, 1997]. However, over most of the tropical oceans this record of data is not yet in existence.

[5] Global satellite data at an appropriate temporal and spatial resolution are available during the past several years. The Global Precipitation Climatology Project's (GPCP) one-degree daily (1DD) data set [Huffman et al., 2001] is a homogeneous and continuous record of precipitation for the globe since late 1996. The Tropical Rainfall Measuring Mission (TRMM) has provided the highest-quality and highest-resolution precipitation and SST estimates from space since 1998 [Kummerow et al., 2000]. Scatterometer measurements aboard QuikSCAT have yielded globally gridded fields of sea surface wind vectors since 1999 [Spencer et al., 2000]. These products allow for detailed case studies of daily variations in the tropical oceans and atmosphere over entire seasons, leading to new insights into coupled processes. For example, Harrison and Vecchi [2001] used TRMM SST data to examine a rapid cooling in the tropical Indian Ocean during January 1999. The observed cooling was preceded by strong westerly winds south of the equator.

[6] Here we examine the climate of the eastern Indian Ocean following Curtis et al. [2002], who identified a relationship between both MJO-type oscillations and seasonal shifts in wind/precipitation anomalies and the subsequent initiation of El Niño events in the Pacific Ocean. The potential of developing a prediction index based on both the intraseasonal and seasonal variations of wind and the limited amount of skill of current statistical and coupled ocean-atmosphere models in predicting El Niño [Landsea and Knaff, 2000] motivate this investigation with high-resolution, high-quality satellite-based data sets. In section 2 we give a background on climate features of the eastern Indian Ocean. We also define an appropriate WWB domain in the near-equatorial southern Indian Ocean and examine the interannual variability of number of WWB days. In section 3 we develop a precipitation-based prediction index for the onset of El Niño and apply it to the period 1979–2003. In section 4 high-resolution observations of

rain, wind, and SST from the Indian to Pacific Ocean in the austral summer season preceding the 2002–2003 El Niño are presented in order to identify air-sea linkages between the basins.

2. Climate Features of the Eastern Indian Ocean

[7] Long-term climatologies of NCEP/NCAR reanalysis 1000 mbar zonal wind [Kalnay et al., 1996] and GPCP Version 2 precipitation [Adler et al., 2003] in the Indian Ocean are shown for September, November, January, and March (Figure 1), encompassing the Australian monsoon season. Precipitation associated with the Indian Ocean Convergence Zone is consistently found south of the equator and is most intense in January (Figure 1c). Westerly winds in the northern Indian Ocean in September (Figure 1a) move southward until January (Figure 1c). For the austral summer season the strongest gradient of zonal wind occurs between 5° and 15°S, suggesting a favored area of vorticity and storm generation. This is also consistent with Figure 2, which is the second-strongest combined EOF pattern of 1000 mbar wind and precipitation for the Indian Ocean [Curtis et al., 2002]. Figure 2 shows a gradient of precipitation anomalies across the equator and strong westerly wind anomalies centered around 95°E and 5°S. The wind anomalies decrease to the south, reaching zero at 15°S. For these reasons, WWB events were defined for the box in Figure 1 (5°–15°S; 70°–100°E).

[8] Studies of the climate of the western Pacific [Harrison and Vecchi, 1997; Yu and Rienecker, 1998] connect WWB events to storms and precipitation. Similarly in the near-equatorial southern Indian Ocean strong westerly winds could be generated on the northern flank of tropical cyclones or to the west of convective complexes. Intraseasonal to interannual variations in the precipitation gradient seen in Figure 2, have been shown to precede the onset of El Niño [Curtis et al., 2002]. Considering the relationship between zonal wind and precipitation in the combined EOF, WWBs as defined below may also be a good predictor for El Niño.

[9] First, monthly climatologies (1979 to 2002) of WWB event days were computed. A WWB event day was defined as a day when the NCEP 1000 mbar zonal wind was greater than +1.5 standard deviations from the mean, which accounts for less than 8% of the total number of days. The numbers of event days for September–October–November from 1979 to 2001 and January–February–March from 1980 to 2002 are presented in Figure 3 (solid circles). Large numbers of WWB event days occurred prior to the onsets of the 1982–1983, 1991–1992, 1997–1998, and 2002–2003 El Niño events (Figure 3). The onset is defined as the date when the three-month average of Nino 3.4 is greater than 0.5°C. Overall, the 1996–1997 season contained the largest number of WWB event days, with the bulk (23) occurring from September to November (Figure 3a). The largest number of WWB event days from January to March occurred during 2002 (Figure 3b). However, WWB event days were near normal prior to the 1986–1987 El Niño and were numerous at other times when no El Niño occurred. The number of westerly wind burst days for each month (September to April) was sorted on the basis of the December (year +1) value of Nino 3.4. September was the only

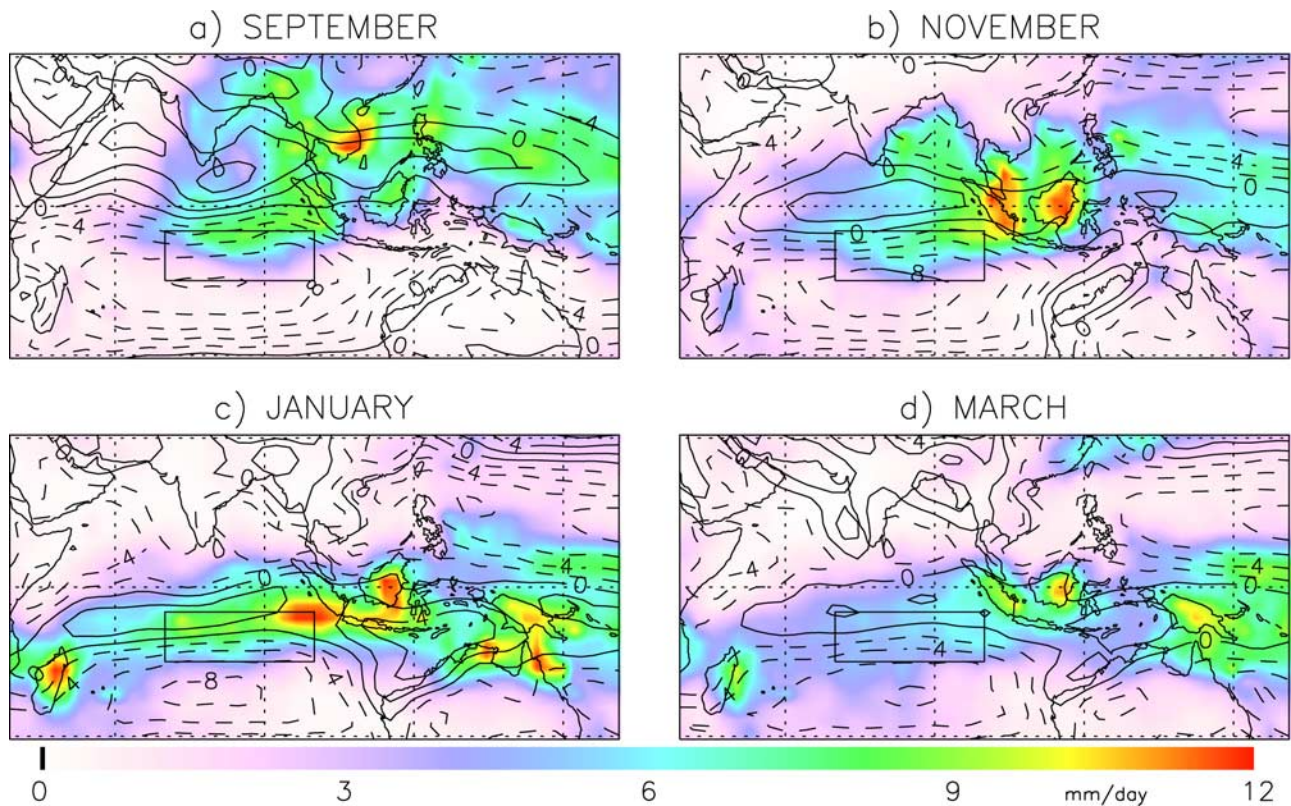


Figure 1. Climatologies of 1000 mbar zonal wind (contours) and precipitation (shading). Contours are every 2 m s⁻¹. Box (5°–15°S; 70°–100°E) indicates area used to define westerly wind burst events. (a) September, (b) November, (c) January, and (d) March.

month to have significantly different (at the 90% level) numbers of WWB event days for El Niño (Nino 3.4 in excess of 0.5°C) versus years that were not El Niño years.

[10] The weak relationship between WWB event days in the Indian Ocean and onset of El Niño is somewhat surprising considering Figure 2, and the results of Curtis *et al.* [2002], which related variations in precipitation gradient (in turn related to surface wind) to El Niño. One reason may be the reliability of the surface wind in the reanalysis [Goswami and Sengupta, 2003]. Interestingly, the largest numbers of WWB event days occurred before the last two El Niño events. The later part of the wind record likely has a higher quality and quantity of assimilated observations. Previous studies (see section 1) also indicate that mean wind/precipitation conditions play a role in the Indian Ocean–El Niño relation. This will be explored further in the next section.

3. Precipitation-Based El Niño Onset Index (EOI)

[11] Considering the lack of skillful predictability with the WWB information, a near-real-time El Niño Onset Index (EOI), based solely on GPCP pentad precipitation data [Xie *et al.*, 2003] was developed, following the work of Curtis *et al.* [2002]. The relationship is reasonable considering the link between precipitation gradient and surface wind in the eastern Indian Ocean (Figure 2). Using the time series of the gradient of precipitation anomalies in the eastern Indian Ocean (east box minus west box, Figure 2), significant power in the 30–60 day band of a wavelet

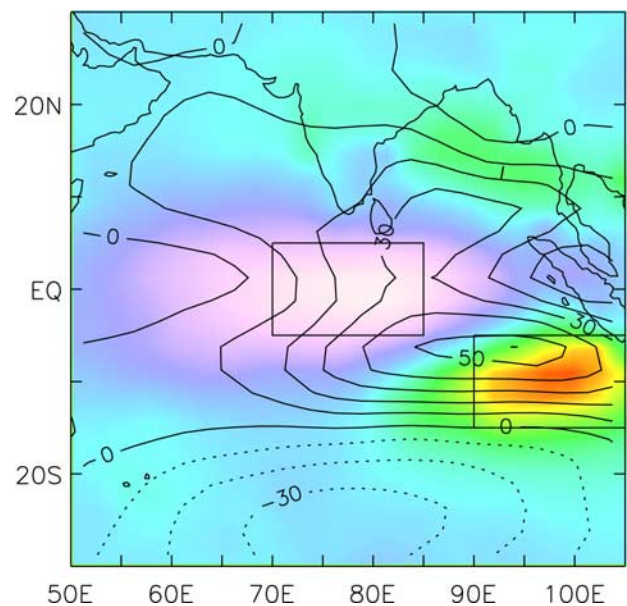


Figure 2. The second combined EOF of precipitation, 1000 mbar zonal wind, and 1000 mbar meridional wind anomalies in the Indian Ocean sector from 1979 to 1999. The precipitation is shaded, and the zonal wind is shown in contours (units are arbitrary). Boxes indicate areas used to define the pronounced gradient in precipitation anomalies. After Curtis *et al.* [2002, Figure 1b].

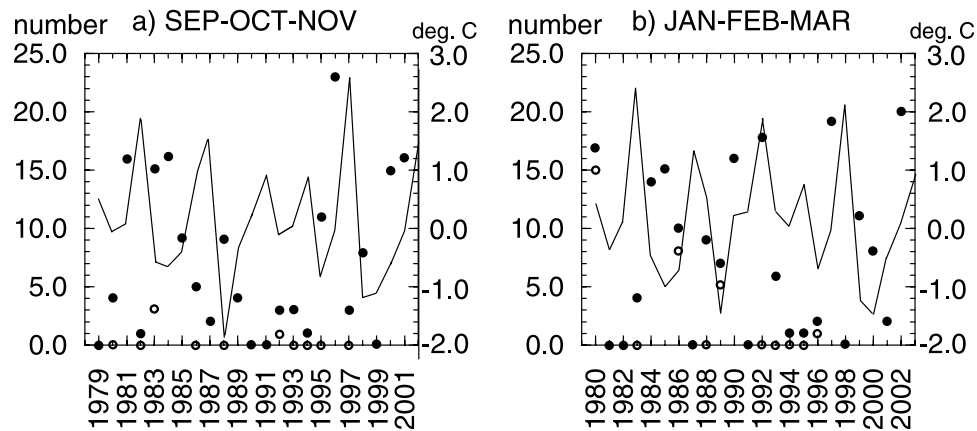


Figure 3. Solid circles denote number of westerly wind burst (WWB) days (scale is left) over the box shown in Figure 1 for (a) September–October–November 1979–2001 and (b) January–February–March 1980–2002. Data are daily NCEP/NCAR reanalysis 1000 mbar zonal wind anomalies. A WWB day is defined as having a wind value greater than +1.5 standard deviations. Open circles are a subset of WWB days when the trailing six-month mean of the zonal wind anomaly is westerly. The curve is Nino 3.4 (scale in $^{\circ}\text{C}$ is right) averaged over the three months.

analysis is determined as the key parameter in relation to occurrence of El Niño. Curtis *et al.* [2002] also showed that a second parameter, the 2–7 year filtered time series of the precipitation gradient, associated with anomalous westerly surface flow, helps eliminate false positives. Thus this earlier work showed a clear link between combined conditions in the eastern Indian Ocean of (1) high energy in 30–60 day variations in climate and (2) long-term average conditions similar to Figure 2 and the subsequent occurrence of El Niño.

[12] To convert these relations to a prediction index, the 2–7 year filtered time series was replaced by a simple trailing six-month mean of the gradient of precipitation anomalies. The result of the EOI calculation is shown in Figure 4, a measure of the 30–60 day power in zonal surface wind (using the precipitation proxy). Black (gray)

areas indicate pentads that have a positive (negative) trailing six-month mean value of the gradient of precipitation anomalies. Thus the peaks of the black areas represent strong 30–60 day oscillation activity that occurs following seasons of anomalous westerly wind. An El Niño forecast is made when the black area exceeds $14 (\text{mm d}^{-1})^2$. The threshold was set to this high (>90th percentile) value because it captures as many of the El Niño events as possible while minimizing the occurrences of false positives. During the developmental period (1979 to 1999) the threshold of $14 (\text{mm d}^{-1})^2$ yielded one missed event (the 1993 El Niño) out of six and no false positives. The five successful forecasts preceded El Niños by 5 to 15 months (Figure 4 and Table 1). This range can somewhat be explained by the chosen definition of El Niño onset [Trenberth, 1997]. For example, if the onset is defined as

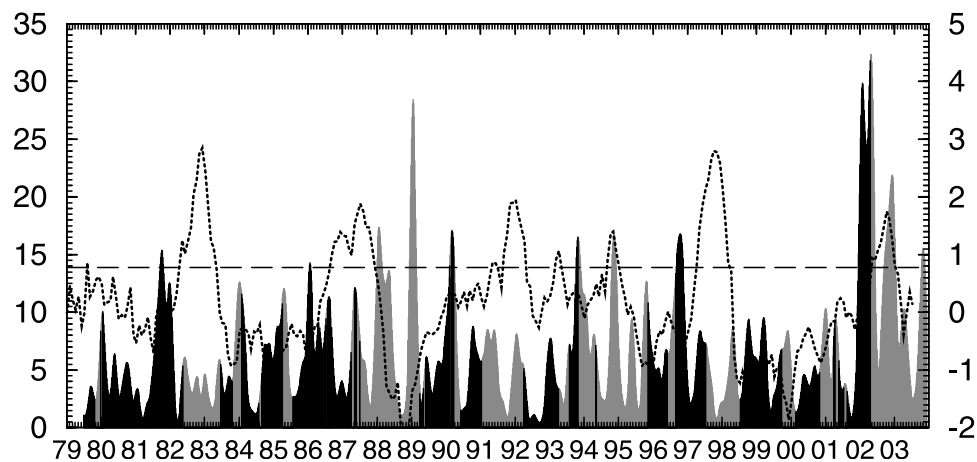


Figure 4. El Niño Onset Index (EOI), namely, the 30–60 day power in $(\text{mm d}^{-1})^2$ (scale at left) of a wavelet analysis of the gradient of precipitation anomalies (see Figure 1). Black (gray) areas indicate pentads that have a positive (negative) trailing six-month mean of the gradient of precipitation anomalies. Only black areas above the 92% significance level (dashed line) yield a positive onset forecast. Thick dotted line is the Nino 3.4 sea surface temperature anomaly in $^{\circ}\text{C}$ (scale at right).

Table 1. Relationship Between the EOI and Onset of El Niño^a

| Maximum EOI | El Niño Onset | Difference, months |
|-------------|---------------|--------------------|
| Sept. 1981 | May 1982 | 8 |
| Jan. 1986 | Sept. 1986 | 8 |
| Feb. 1990 | May 1991 | 15 |
| Oct. 1993 | Sept. 1994 | 11 |
| Sept. 1996 | May 1997 | 8 |
| Dec. 2001 | May 2002 | 5 |

^aUsing standard definition of the three-month average of Nino 3.4 greater than 0.5°C. EOI, El Niño Onset Index.

the date when the three-month average of Nino 3.4 is greater than 0.35° (instead of 0.5°C), the range decreases to 5 to 10 months.

[13] The EOI became operational in 2001, and in early February 2002 it was found that the 21–25 January 2002 value met the necessary conditions for an onset forecast. In fact, the austral summer season of 2001–2002 contains the largest EOI values in the record (Figure 4). The resulting El Niño forecast was reported in March 2002 [Perkins, 2002], prior to any clear consensus that an El Niño was imminent [McPhaden, 2004].

[14] The physical basis for the EOI is explored below. We propose that the aforementioned localized 30–60 day variations in convection are combined with a mean condition of above average westerly wind anomaly, conducive to rapid eastward propagation and successful translation of the MJO into the Pacific Ocean. To test this, the numbers of westerly wind burst days were filtered by the mean condition. Following the approach used to distinguish predictive EOI values (Figure 4), open circles in Figure 3 denote WWB days when the trailing six-month average zonal wind anomaly was positive. This eliminates two false positives in particular: September–October–November 1983 and January–February–March 1992. Furthermore, intraseasonal anomalies of convection coupled to wind and SST [Shinoda *et al.*, 1998; Woolnough *et al.*, 2000] propagating from the Indian Ocean to western Pacific appear to be important for El Niño development. Figure 5 shows the first eigenvector of a complex principal component analysis of GPCP pentad precipitation anomalies for 1979–2001. The largest variance in the subseasonal precipitation occurs on either side of the Maritime Continent, but the variance in the eastern Indian Ocean leads and is approximately in quadrature to

the variance in the western Pacific. It is unclear from the coarse resolution ($2.5^\circ \times 2.5^\circ$) data used in the analysis if the precipitation has a preferred track through the Maritime Continent. In the next section we examine atmospheric and oceanic climate variations in the Indo-Pacific sector during the first and only period of positive EOI forecast, the austral summer of 2001–2002, that falls within the short record of high-resolution satellite data.

4. Case Studies

[15] Intraseasonal climate variations from November 2001 to April 2002 were examined using the one-degree daily (1DD) precipitation data, QuikSCAT wind data, and TRMM microwave imager SST data. Wind and SST at 0.25 degree daily resolution were obtained from F. Wentz at Remote Sensing Systems. Only the u -component of wind was used for this study. All data sets were subjected to a 3-day smoother.

[16] Figure 6 shows daily time series of zonal wind, precipitation, and SST averaged over the box in Figure 1 for 2001–2002 and climatology. The daily wind climatology (thick line in Figure 6a) was constructed from NCEP 1000 mbar daily zonal winds from 1979 to 2001. Consistent with Figure 1, the start of November is characterized by strong easterly winds (6 m s^{-1}), which weaken until becoming westerly for a few days in February. The winds then become easterly again, reaching speeds of 5 m s^{-1} by the end of April.

[17] Daily estimates of wind from satellites (dashed line in Figure 6a) are compared to those from NCEP (solid line in Figure 6a), which were used to construct the WWB climatologies. The data sets correlate at 0.98. This is encouraging since the scatterometer data are not assimilated into the NCEP/NCAR model. A WWB occurred in November–December 2001 and again in January–February 2002. The daily precipitation climatology (thick line in Figure 6b) is an interpolation of the 1979–1998 GPCP Version 2 monthly climatology. The 1DD and Version 2 data sets are consistent in that the 1DD was constructed to add up to the monthly GPCP value [Huffman *et al.*, 2001]. Unlike the wind climatology, it shows a weak seasonal cycle with slightly more rain in January–February than in November–December and March–April. The SST climatology (thick line in Figure 6c), plotted every five days, is a blend of ship

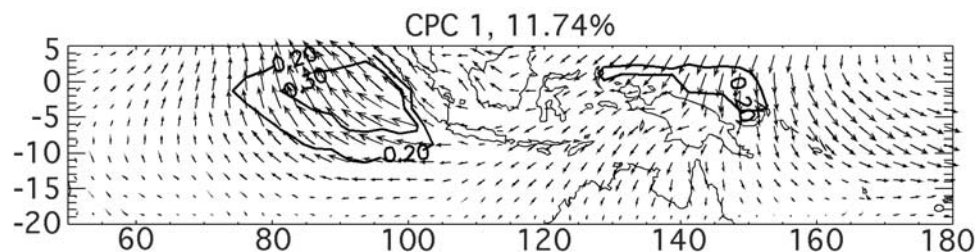


Figure 5. First eigenvector from a complex principal component analysis of GPCP pentad precipitation from 1979 to 2001 (explains 11.74% of the variance). A vector is plotted at each grid box so that its length is proportional to its magnitude and its angle is proportional to its relative phase. Propagation occurs in the direction of counterclockwise rotation. Contours denote the 0.2 and 0.3 levels of local variance explained.

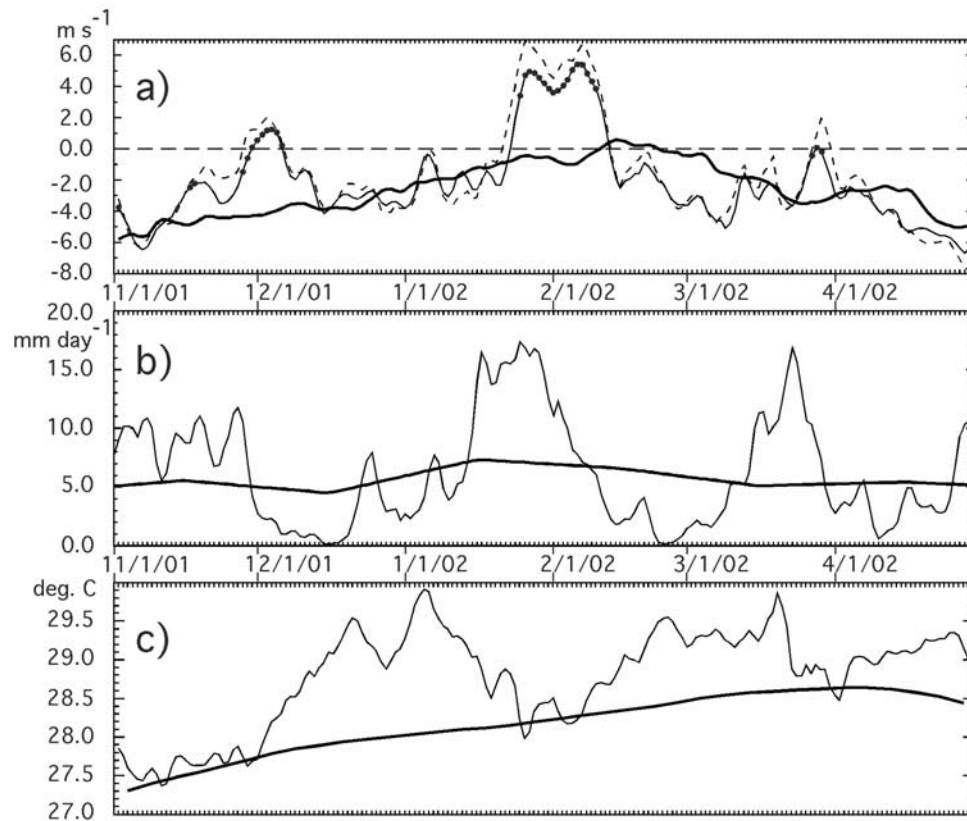


Figure 6. November 2001 to April 2002 time series of daily zonal wind, precipitation, and SST values averaged over the box shown in Figure 1. (a) NCEP/NCAR 1000 mbar zonal wind (thin solid line), zonal wind climatology (thick solid line), and QuikSCAT sea surface zonal wind (thin dashed line). (b) precipitation (thin solid line) and precipitation climatology (thick solid line). (c) SST (thin solid line) and pentad SST climatology (thick solid line). Solid circles in Figure 6a indicate westerly wind burst days.

observations and satellites [Reynolds and Smith, 1994]. This independent climatology is meant to show that SST increases during this part of the annual cycle.

[18] Interestingly, in December-January the ocean surface was warmer than normal, followed by copious precipitation, which led a WWB event (Figure 6). From November 2001 to April 2002 the correlation between 1DD precipitation and QuikSCAT wind reached a maximum of 0.71 when the rainfall led by 9 days. This is consistent with our hypothesis that precipitation can be used as a proxy for the strong westerly winds. Over that same time period the SST-precipitation correlation was 0.57 when SST led precipitation by 27 days. This suggests a coupling with the surface ocean. Both of these correlations are significant at the 99% level.

[19] Next we examine the Indo-Pacific climate system during the November 2001 to April 2002 time period. Particular attention is focused on why the WWB events and associated climate anomalies occurred in the eastern Indian Ocean (Figure 6), and if and how they are communicated to the western Pacific (as is suggested by Figures 4 and 5). Jones *et al.* [2004] also raise the question as to the environmental factors that may distinguish intraseasonal convective anomalies that remain in the Indian Ocean from those that propagate eastward. Figure 7 shows variable-latitude time-longitude diagrams of zonal wind, precipitation, and SST anomalies. A

running 10 degree latitude average was computed from 20°S to 15°N for each variable. The maximum value, plotted in Figure 7, represents the strongest climate signal within the deep tropics. The two longest periods of WWB days (Figure 6a) are depicted as boxes in the left panel. Two eastward propagating wind-rain systems occur in November-December and January-February (Figure 7, left panel). Interestingly, the first propagating system appears to be east of 100°E at the time of the WWB event. This relationship will be explored further below.

[20] In the second event the wind-rain system moves through the WWB box (Figure 7, left panel). The SST data shows quite strikingly a warming between 60° and 80°E that lasted a few days in early January (Figure 7, right panel). The warming may have initiated, after some lag time, the convection that traveled to the western Pacific. The waters also warmed (cooled) before (after) the passage of the wind-rain system from 120°E to 180° (Figure 7, right panel).

[21] It is interesting to note that wind and precipitation travel eastward in bursts (Figure 7), rather than in a smooth progression. The longitude of the heaviest rainfall in Figure 7 was recorded each day. For the time period of the two systems, the locations of the precipitation maxima are shown in Figure 8. The locations of the wind maxima for the same dates are shown as well. For the first system (Figure 8a) a

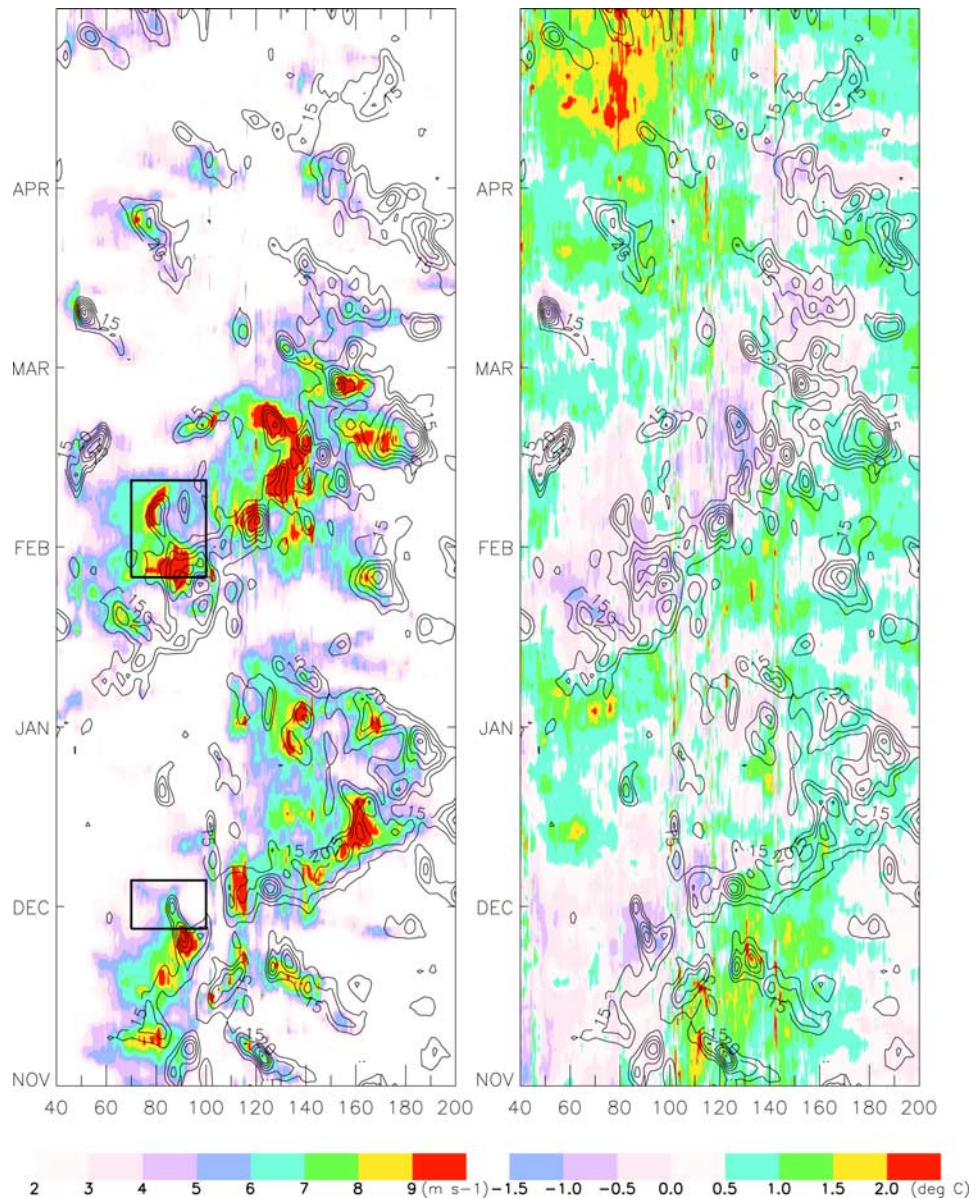


Figure 7. Variable time-longitude diagrams of zonal wind, rainfall, and SST anomaly for 40°E to 160°W and from November 2001 to April 2002. The maximum value of a running 10 degree latitude average from 20°S to 15°N is plotted for each variable. (left) QuikSCAT overlain with contours of 1DD precipitation (15, 20, 25, 30, 35, 40, and 45 mm d^{-1}). (right) TRMM SST anomalies, derived by subtracting each point by its longitudinal average, overlain with contours of 1DD precipitation (15, 20, 25, 30, 35, 40, and 45 mm d^{-1}). Boxes denote the times of westerly wind bursts.

heavy rain event on 27 November was located within the area used to define WWBs (see box) accompanied by strong westerly winds just south of the equator. The next precipitation maximum on 5 December was centered over the Philippines, as the strongest wind was located further west over Borneo. On 11 and 18 December the wind and precipitation are nearly collocated in the western Pacific.

[22] For the second system (Figure 8b), the first precipitation maximum occurred on 27 January near Sumatra. The strongest wind on that date was found within the box used to define WWBs. This wind-rain system took a track along the north coast of Australia. On 4 February the precipitation

and wind maxima were collocated in the North Australian basin. However, the 10 February precipitation maximum appeared east of Australia, while the strongest wind lagged behind near 130°E . On 17 February the precipitation maximum was within the South Pacific Convergence Zone, but at the same time the wind maximum remained on the north coast of Australia. On 26 February another precipitation maximum was located north of the equator accompanied by strong equatorial westerlies. While the two propagating systems would be considered equatorial, they clearly take different tracks from the Indian to the Pacific Oceans, with the second clearly south of the equator, via the

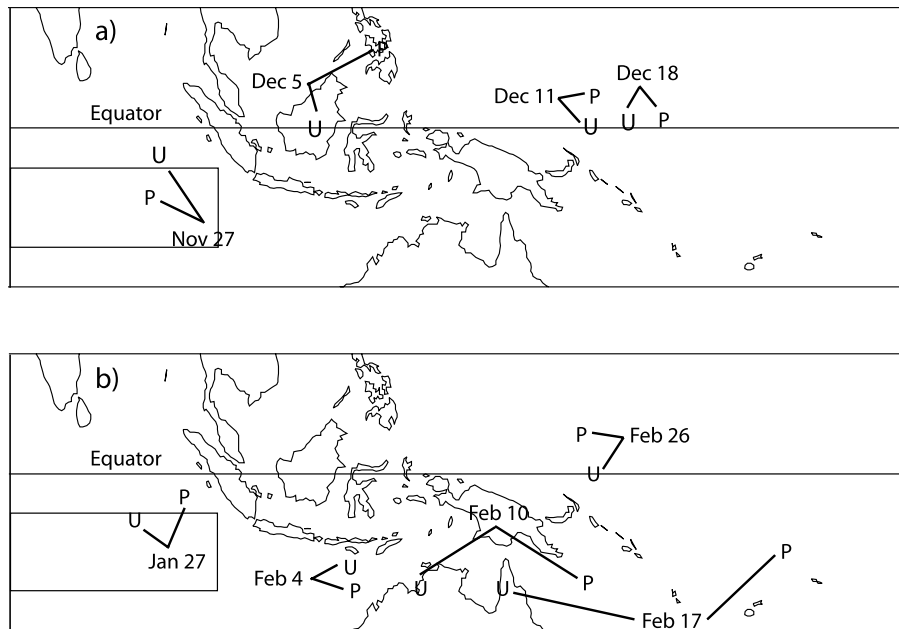


Figure 8. (a and b) Locations of maximum values of precipitation “P” in Figure 7 (left panel) for selected days. Maximum values of zonal wind “U” are plotted for the same days. Box (5° – 15° S; 70° – 100° E) indicates area used to define westerly wind burst events.

Timor Strait. The fact that this event tracked almost entirely over ocean may explain the apparently strong coupling with SST in Figure 7, right panel.

[23] While Figures 6–8 give an encapsulated summary of intraseasonal climate features of the 2001–2002 season, selected maps of precipitation, zonal wind, and SST are presented for completeness. Figure 9 shows the state of the Indo-Pacific sector for 27 and 30 November and 3 and 6 December. The succession of maps is consistent with the locations of rainfall and wind maxima during these days (Figure 8a). On 27 November the strongest winds are on the equator in the eastern Indian Ocean, while the heaviest rainfall is further south over the study area. The bulk of the enhanced westerly winds and rainfall move to the north (as in Figure 8a). However, there is a center of precipitation, associated with tropical cyclone Bessi-Bako, that travels to the south (Figure 9). Thus strong westerly winds on the north side of the cyclone pass through the study area (Figures 9b, 9c, and 9d) resulting in a 9-day WWB event (Figure 6).

[24] The second WWB event in January–February (Figure 6) coincides with eastward propagation of strong wind and heavy precipitation (Figures 7 and 8b). However, prior to any organization in winds and rainfall (Figure 10a), high sea surface temperatures are found in a band across the Indian Ocean on 5 January (Figure 10b). Voids in the SST estimates occur when TMI detects precipitation. These areas are generally located within the largest 1DD precipitation contours. As precipitation builds in the central Indian Ocean (Figure 10c), the basin cools (Figure 10d). On 19 January, strong westerly winds and heavy precipitation stretch from Sumatra to Madagascar (Figure 10e), while SSTs increase between Indonesia and Australia (Figure 10f). Tropical cyclone Dina is observed near 60° E (Figure 10e). On 26 January, two centers of rainfall are located to the west of Sumatra and in the southern Indian Ocean (Figure 10g). The

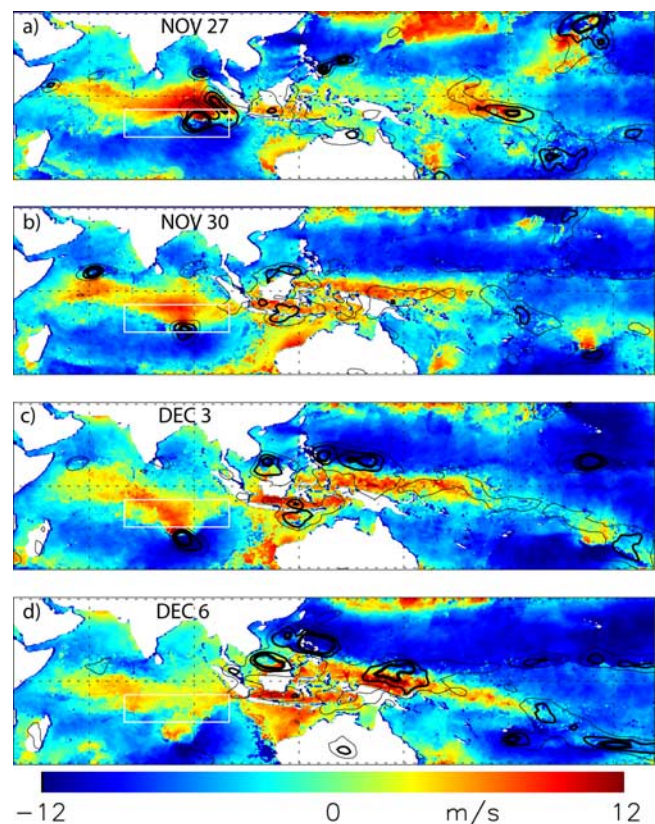


Figure 9. (a–d) Three-day averages of zonal wind from QuikSCAT overlain with contours of 1DD precipitation (10 , 20 , and 30 mm d^{-1}) for a period in late November and early December 2001.

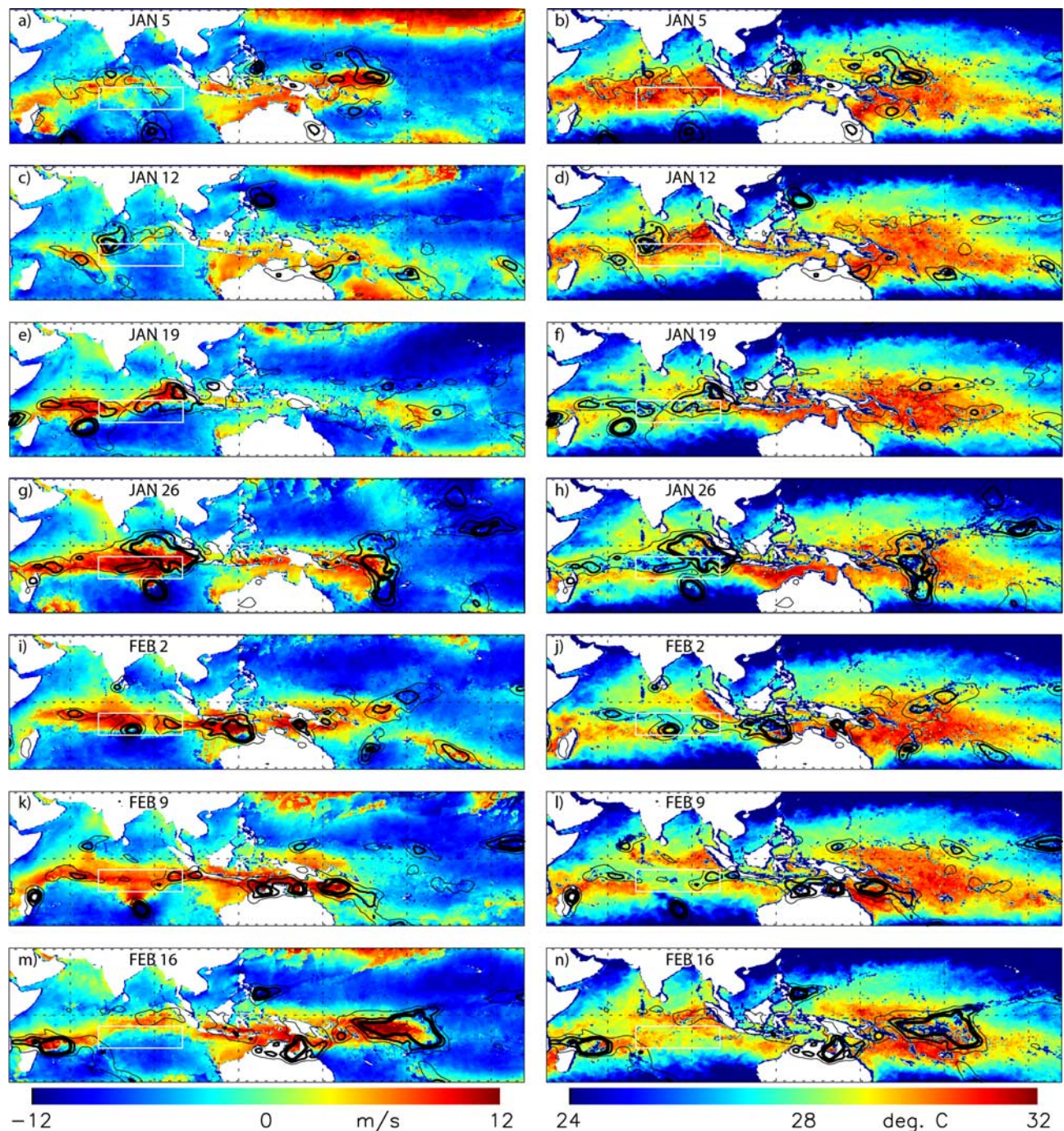


Figure 10. (a–n) Three-day averages of zonal wind from QuikSCAT (left panels) and SST from TRMM (right panels) overlain with contours of 1DD precipitation ($10, 20, \text{ and } 30 \text{ mm d}^{-1}$) for a period in January and February 2002.

later is associated with tropical cyclone Eddy. This combination is accompanied by strong westerly winds in the study area. The heaviest rainfall is to the north of the winds, consistent with Figure 8b. The wind-rain system moves swiftly eastward over the warmer waters on 2 February (Figure 10i), leaving cooler waters in its wake (Figure 10j). At this time the warmest surface waters are found to the east of the rainfall and winds in the Coral Sea (Figure 10j). On 9 February the precipitation and westerly winds push across the north coast of Australia, while tropical cyclone Francesca

contributes to strong westerly winds over the study region (Figure 10k). The prevalence of tropical cyclones during this period is consistent with other studies linking enhanced tropical storm activity with the passage of the MJO [Maloney and Hartmann, 2000a, 2000b; Higgins and Shi, 2001]. SSTs increase over the western equatorial Pacific and decrease over the North Australian basin (Figure 10l). On 16 February the propagating system reaches the western Pacific and wind speeds above 10 m s^{-1} extend to the dateline. At the same time wind speeds diminish over the eastern Indian Ocean

(Figure 10m). This sequence of maps (Figure 10) suggests a strong coupling of precipitation, winds, and SST.

[25] This case study clearly shows that twice during the 2001–2002 EOI forecast period wind, rain, and SST anomalies tracked from the Indian to Pacific Ocean. While this propagation is likely associated with the MJO, high-resolution satellite data shows imbedded bursts of wind and rainfall associated with tropical cyclones. Also, the strongest wind and rain signals in the second system track south of the equator through the Timor Strait.

5. Discussion and Conclusions

[26] This paper uses both climatological and state-of-the-art satellite estimates of precipitation and wind to better develop and understand previous studies linking intraseasonal to seasonal climate variability in the eastern Indian Ocean to the onset of El Niño. First, this paper extends previous work compiling westerly wind burst (WWB) climatologies in the western Pacific to include the eastern Indian Ocean during austral summer. A large interannual variability in WWB days was noted, with peaks before some, but not all El Niño events. Second, this paper develops an El Niño Onset Index (EOI) based on rainfall variability in the eastern Indian Ocean for the prediction of the onset of El Niño. The EOI relies on detecting periods of peak westerly wind activity in the 30–60 day window that occur during periods of mean conditions associated with strong westerly winds. The index uses precipitation information for its basis because of a stronger signal in that variable, due to the relatively higher quality satellite observations of convection and precipitation during the last 25 years. The EOI was shown to reach high levels before almost all the El Niño events from 1979 to 1999. The EOI also reached significant values during the austral summer of 2001–2002, successfully forecasting the 2002–2003 El Niño. Advances in the real time application of the EOI are being made with high-time-resolution multisatellite precipitation analyses, which use the Tropical Rainfall Measuring Mission (TRMM) to calibrate or adjust the rainfall information from polar-orbiting and geosynchronous satellites.

[27] The EOI requires periods of high 30–60 day variability in the zonal wind combined with a background of above average westerly wind anomaly. We suggest that this combination is conducive to a rapid eastward propagation and successful translation of intraseasonal convective anomalies from the Indian Ocean to the Pacific Ocean. The processes imbedded in the success of the EOI need additional analysis and model-based simulation of the connection between the events in the Indian Ocean and subsequent events in the Pacific Ocean.

[28] The 2001–2002 EOI forecast period was examined in detail with satellite observations of precipitation, wind, and SST to better understand these linkages. Twice, convection, along with localized variations in wind and SST, propagated along a complicated, and not necessarily equatorial, path from the Indian Ocean to the western Pacific, where wind-sea interactions are important for El Niño development. These paths appear to be imbedded within the larger MJO structure [e.g., *Rui and Wang*, 1990]. We speculate that the convection is coupled with the ocean

surface and is steered by the warmest waters during the annual cycle. Thus a track on the equator may be less favorable, because of the large islands of Sumatra and Borneo. Of the two propagating systems, the second is more convincingly coupled with the SST. Beginning in January 2002, heavy rains led strong westerly winds by 9 days in the eastern Indian Ocean. The wind-rain system moved over the waters between Indonesia and Australia and into the western Pacific about three weeks later (from approximately 26 January to 16 February). Warm waters in the eastern Indian Ocean appeared about a month before the heaviest precipitation, but were not well correlated with the westerly winds, suggesting that the warming does not induce WWBs directly, but through the generation of convection. The warm waters continued to lead rainfall to the north of Australia, and into the Pacific.

[29] The case studies presented here with high-resolution satellite data are intriguing considering the success of the EOI. Zonal wind stress in the western Pacific, with appropriate seasonal mean and intraseasonal frequencies, can directly affect El Niño. We have shown that for the 2001–2002 season strong westerly winds in the western Pacific can be traced back to the eastern Indian Ocean. This is consistent with a complex principal component analysis of precipitation anomalies in the Indo-Pacific sector, which shows variations in the eastern Indian Ocean leading variations in the western Pacific. It is proposed that air-sea coupling acts as a bridging mechanism between the two basins by intensifying and propagating atmospheric disturbances from the Indian to Pacific Ocean.

[30] **Acknowledgments.** The authors would like to thank Chris Landsea and two other anonymous reviewers for their constructive comments. This work is supported by a grant from NASA's Precipitation Missions Science Program, which includes the Tropical Rainfall Measuring Mission (TRMM). The authors would like to thank Remote Sensing Systems, who produced the TMI SST data, sponsored by NASA's Earth Science Information Partnerships (ESIP); a federation of information sites for Earth Science; and by NASA's TRMM Science Team, and QuikSCAT data, sponsored by the NASA Ocean Vector Winds Science Team. Finally, the authors are indebted to Alberto Mestas Nunez and David Enfield for supplying the Complex Principal Component Analysis code and for their help in interpreting the results.

References

- Adler, R. F., et al. (2003), The Version 2 Global Precipitation Climatology Project (GPCP) monthly precipitation analysis (1979–present), *J. Hydrometeorol.*, **4**, 1147–1167.
- Belamari, S., J. L. Redelsperger, and M. Pontaud (2003), Dynamic role of a westerly wind burst in triggering an equatorial Pacific warm event, *J. Clim.*, **16**, 1869–1890.
- Clarke, A. J., and S. Van Gorder (2003), Improving El Niño prediction using a space-time integration of Indo-Pacific winds and equatorial Pacific upper ocean heat content, *Geophys. Res. Lett.*, **30**(7), 1399, doi:10.1029/2002GL016673.
- Curtis, S., G. J. Huffman, and R. F. Adler (2002), Precipitation anomalies in the tropical Indian Ocean and their relation to the initiation of El Niño, *Geophys. Res. Lett.*, **29**(10), 1441, doi:10.1029/2001GL013399.
- Fedorov, A. V. (2002), The response of the coupled tropical ocean-atmosphere to westerly wind bursts, *Q. J. R. Meteorol. Soc.*, **128**, 1–23.
- Fedorov, A. V., S. L. Harper, S. G. Philander, B. Winter, and A. Wittenberg (2003), How predictable is El Niño?, *Bull. Am. Meteorol. Soc.*, **84**, 911–919.
- Goswami, B. N., and D. Sengupta (2003), A note on the deficiency of NCEP/NCAR reanalysis surface winds over the equatorial Indian Ocean, *J. Geophys. Res.*, **108**(C4), 3124, doi:10.1029/2002JC001497.
- Gutzler, D. S., and D. E. Harrison (1987), The structure and evolution of seasonal wind anomalies over the near-equatorial eastern Indian and western Pacific Oceans, *Mon. Weather Rev.*, **115**, 169–192.

- Harrison, D. E., and N. K. Larkin (1998), El Niño–Southern Oscillation sea surface temperature and wind anomalies, 1946–1993, *Rev. Geophys.*, *36*, 353–399.
- Harrison, D. E., and G. A. Vecchi (1997), Westerly wind events in the tropical Pacific, 1986–95, *J. Clim.*, *10*, 3131–3156.
- Harrison, D. E., and G. A. Vecchi (2001), January 1999 Indian Ocean cooling event, *Geophys. Res. Lett.*, *28*, 3717–3720.
- Higgins, R. W., and W. Shi (2001), Intercomparison of the principal modes of interannual and intraseasonal variability of the North American Monsoon System, *J. Clim.*, *14*, 403–417.
- Huffman, G. J., R. F. Adler, M. Morrissey, D. T. Bolvin, S. Curtis, R. Joyce, B. McGavock, and J. Susskind (2001), Global precipitation at one-degree daily resolution from multi-satellite observations, *J. Hydrometeorol.*, *2*, 36–50.
- Jones, C., L. M. V. Carvalho, R. W. Higgins, D. E. Waliser, and J.-K. E. Schemm (2004), Climatology of tropical intraseasonal convective anomalies: 1979–2002, *J. Clim.*, *17*, 523–539.
- Kalnay, E., et al. (1996), The NCEP/NCAR 40-year reanalysis project, *Bull. Am. Meteorol. Soc.*, *77*, 437–471.
- Kessler, W. S., and R. Kleeman (2000), Rectification of the Madden-Julian oscillation into the ENSO cycle, *J. Clim.*, *13*, 3560–3575.
- Krishnamurti, T. N., D. Bachiochi, T. LaRow, B. Jha, M. Tewari, D. R. Chakraborty, R. Correa-Torres, and D. Oosterhof (2000), Coupled atmosphere-ocean modeling of the El Niño of 1997–98, *J. Clim.*, *13*, 2428–2460.
- Kummerow, C., et al. (2000), The status of the Tropical Rainfall Measuring Mission (TRMM) after two years in orbit, *J. Appl. Meteorol.*, *39*, 1965–1982.
- Landsea, C. W., and J. A. Knaff (2000), How much skill was there in forecasting the very strong 1997–98 El Niño?, *Bull. Am. Meteorol. Soc.*, *81*, 2107–2119.
- Madden, R. A., and P. R. Julian (1994), Observations of the 40–50 day tropical Oscillation: A review, *Mon. Weather Rev.*, *122*, 814–835.
- Maloney, E. D., and D. L. Hartmann (2000a), Modulation of hurricane activity in the Gulf of Mexico by the Madden-Julian oscillation, *Science*, *287*, 2002–2004.
- Maloney, E. D., and D. L. Hartmann (2000b), Modulation of eastern North Pacific hurricanes by the Madden-Julian oscillation, *J. Clim.*, *13*, 1451–1460.
- McPhaden, M. J. (2004), Evolution of the 2002/03 El Niño, *Bull. Am. Meteorol. Soc.*, *85*, 677–695.
- Perkins, S. (2002), El Niño's coming! Is that so bad?, *Sci. News*, *161*, 142.
- Reynolds, R. W., and T. M. Smith (1994), Improved global sea surface temperature analyses using optimum interpolation, *J. Clim.*, *7*, 929–948.
- Rui, H., and B. Wang (1990), Developmental characteristics and dynamic structure of tropical intraseasonal convection anomalies, *J. Atmos. Sci.*, *47*, 357–379.
- Shinoda, T., H. H. Hendon, and J. Glick (1998), Intraseasonal variability of surface fluxes and sea surface temperature in the tropical western Pacific and Indian Oceans, *J. Clim.*, *11*, 1685–1702.
- Spencer, M. W., C. L. Wu, and D. G. Long (2000), Improved resolution backscatter measurements with the SeaWinds pencil-beam scatterometer, *IEEE Trans. Geosci. Remote Sens.*, *38*, 89–104.
- Trenberth, K. E. (1997), The definition of El Niño, *Bull. Am. Meteorol. Soc.*, *78*, 2771–2777.
- Vecchi, G. A., and D. E. Harrison (2000), Tropical Pacific sea surface temperature anomalies, El Niño, and equatorial westerly wind events, *J. Clim.*, *13*, 1814–1830.
- Woolnough, S. J., J. M. Slingo, and B. J. Hoskins (2000), The relationship between convection and sea surface temperature on intraseasonal time-scales, *J. Clim.*, *13*, 2086–2104.
- Xie, P., J. E. Janowiak, P. A. Arkin, R. Adler, A. Gruber, R. Ferraro, G. J. Huffman, and S. Curtis (2003), GPCP pentad precipitation analyses: An experimental data set based on gauge observations and satellite estimates, *J. Clim.*, *16*, 2197–2214.
- Yu, L., and M. M. Rienecker (1998), Evidence of an extratropical atmospheric influence during the onset of the 1997–98 El Niño, *Geophys. Res. Lett.*, *25*, 3537–3540.
- Zhang, C., and J. Gottschalck (2002), SST anomalies of ENSO and the Madden-Julian oscillation in the equatorial Pacific, *J. Clim.*, *15*, 2429–2445.

R. F. Adler, G. Gu, and G. J. Huffman, NASA Goddard Space Flight Center, Code 912, Greenbelt, MD 20771, USA. (adler@agnes.gsfc.nasa.gov; gu@agnes.gsfc.nasa.gov; huffman@agnes.gsfc.nasa.gov)

S. Curtis, Department of Geography, East Carolina University, Brewster A232, Greenville, NC 27858, USA. (curtisw@mail.ecu.edu)